# Dynamics of two-photon double ionization of helium in short intense xuv laser pulses

Xiaoxu Guan,[1] K. Bartschat,[1] and B. I. Schneider[2]
[1]*Department of Physics and Astronomy, Drake University, Des Moines, Iowa 50311, USA*
[2]*Physics Division, National Science Foundation, Arlington, Virginia 22230, USA*
(Received 30 January 2008; published 29 April 2008)

We present an *ab initio* nonperturbative time-dependent approach to the problem of a helium atom driven by an intense xuv laser pulse. Based on the finite-element discrete-variable-representation, a space discretization is proposed for the radial grid in spherical coordinates. Absolute angle-integrated and triple-differential cross sections for double ionization by absorption of two photons are obtained over a range of photon energies between 39.5 eV (31.4 nm) and 54 eV (23 nm), where the process is dominated by nonsequential ionization mechanisms. We show that the agreement with several other sets of previous predictions is good, as long as the effective interaction time is defined properly. Two-photon double ionization at the photon energy of 57 eV (22 nm), for which both sequential and nonsequential channels are open, is also discussed. For double photoionization in the near-threshold regime, our results do not indicate a preferential mode of energy sharing between the two escaping electrons, while asymmetric energy sharing becomes the dominant mode with increasing excess energy. Overall, the two ionized electrons strongly prefer to escape along the polarization axis of linearly polarized laser fields.

DOI: 10.1103/PhysRevA.77.043421 PACS number(s): 32.80.Rm, 32.80.Fb, 42.50.Hz, 32.60.+i

## I. INTRODUCTION

Recent advances in the availability of intense radiation from free-electron laser sources [1–4], which are operating in a wide spectral range, and high-order harmonic generation sources [5] in the extreme ultraviolet (xuv) regime have opened up new avenues to depict the atomic and molecular inner-shell dynamics on an unprecedented ultrashort time scale. Innovative detection techniques, such as COLd Target Recoil-Ion Momentum Spectroscopy (COLTRIMS) [6], have enabled experimentalists to precisely measure the momenta and energies of the particles involved in a complete breakup reaction of few-electron atomic and molecular systems, with He and $H_2$ being the two primary targets of current investigations.

The two-photon double ionization (DI) of the helium atom induced by intense short xuv laser pulses has received considerable attention from both theorists [7–15] and experimentalists [16] over the past few years. The two-photon DI cross section at a photon energy of 41.8 eV was experimentally determined by using an intense xuv pulse produced by high-order harmonics [16]. Theoretically, copious approaches, based upon the time-dependent Schrödinger equation (TDSE) have been developed and refined to depict the two-electron response to a temporal laser pulse. These include the finite-difference methods of Taylor [7], Pindzola, Robicheaux, Colgan [8,9] and their many collaborators, the atomic *B*-spline approach of Bachau and collaborators [10], the *R*-matrix Floquet approach of van der Hart and Feng [11], and the *J*-matrix method of Piraux's group [12]. Very recently, the problem was also addressed by Ivanov and Kheifets [13], who projected the time-propagated wave function on a field-free momentum-space convergent close-coupling (CCC) wave function, and by McCurdy and coworkers [14], who solved coupled Dalgarno–Lewis-type driven equations perturbatively using the exterior complex scaling (ECS) approach, and Shakeshaft [15], who applied second-order perturbation theory.

For xuv radiation with a peak intensity around $10^{14}$–$10^{15}$ W/cm$^2$, the average ponderomotive energy gained by an electron over one optical cycle (o.c.) is considerably smaller than a typical photon energy of about 45 eV. This suggests that the lowest nonvanishing order of perturbation theory (LOPT) should be valid for the two-photon DI process for these situations [17]. Therefore, it is meaningful to define the *N*-photon generalized cross section and to extract its value from the solution to the TDSE, as long as proper care is taken for the intensity, duration, and shape of the laser pulse. If perturbation theory is valid, this cross section can be calculated using effectively time-independent methods (infinitely long pulses). In practical calculations, a small dependence of the extracted cross section on these parameters might occur, but then one has to be careful about the interpretation of such results.

Although our understanding of the problem has certainly improved through the intense efforts mentioned above, there are still many open questions. For the one-photon DI of helium initially in its ground state, good agreement between experiment and theory has been achieved over the entire range of photon energies between threshold [18] and the asymptotic regime [19], where the shake-off process dominates [20]. In contrast to one-photon DI, however, the current situation for two-photon DI of the same system is far from satisfactory. There continue to be active debates as to the importance of final state correlation in the double-continuum state with two free electrons and the residual $He^{2+}$ ion for extracting physically meaningful quantities from the propagated solution of the TDSE. In principle, one should project onto the exact solution to the Schrödinger equation in the absence of the electromagnetic field. In most practical instances, however, this is computationally difficult, and it is worth investigating how simpler approaches affect the extracted cross sections. The published total cross sections for the process (see, for example, Ref. [14]) differ by almost two orders of magnitude depending on how these cross sections are extracted. There are claims in the literature [12] that ac-

 

counting for the full correlation in the final state changes the results dramatically when compared to approaches which project the solution to the TDSE onto an uncorrelated product of two Coulomb functions. From a purely theoretical point of view, this is no different than projecting onto a product of a bound state of $He^+$ and a Coulomb function for single ionization, yet there have been very few questions raised in the literature concerning that approximation.

The major issue, therefore, is how closely the approximate and exact solutions to the TDSE in the absence of the field affect the computed cross sections. While circumspection is important, the current variations among the existing calculations do not seem sensible. Even within the subset of calculations, which project onto an uncorrelated product of two Coulomb functions, there are disagreements up to about a factor of 2 in the total cross sections, and these differences are further emphasized when one looks at theoretical predictions for the fully differential cross sections. In contrast to the issue regarding the importance (or lack thereof) of correlation in the final state, however, one can explain why these smaller differences exist and give sound theoretical arguments about how to bring them into agreement. This issue will be further discussed below.

The present work on the two-photon breakup problem of the helium atom induced by an intense xuv laser pulse is motivated by the unsatisfactory situation described above. For the parameters typically used in or planned for future experimental investigations, we attempt once again to obtain a nonperturbative time-dependent wave-packet solution to the problem. We carefully define the model below and present some consistency and convergence checks to illustrate the numerical accuracy of our results.

Specifically, we employ a combination of the finite element (FE) and discrete-variable-representation (DVR) methods with a time-dependent Arnoldi-Lanczos algorithm. This FE-DVR grid-based approach provides a convenient way to model the laser-atom interaction. In particular, the span of each finite element can easily be adjusted to meet the need of practical problems. In addition, we do not need the field-free atomic eigenstates (except for the initial state) to achieve the time evolution of the system.

The remainder of this paper is structured as follows. In Sec. II, we describe how the FE-DVR method is applied to the laser-driven two-electron atom, with emphasis on the essential differences between the current approach and many other methods to treat the same problem. A procedure to extract the double ionization information from the time-evolved wave packet is also presented. Section III exhibits our results for the total angle-integrated and the fully differential cross sections for two-photon double ionization at a variety of photon energies. We also check the stability of our results against variations of the laser intensity, the pulse length, the spatial mesh, and the number of partial waves included in the expansion of the wave function. Where available, a comparison with other theoretical predictions is made. Finally, we present some conclusions and an outlook in Sec. IV. Unless otherwise indicated, atomic units (a.u.) are used throughout the paper.

## II. THEORY

### A. FE-DVR method of the two-electron system

The essential idea behind the FE-DVR method is to divide the truncated configuration space into finite elements. Each element is then further discretized by properly chosen local Gaussian DVR points. To achieve a smooth representation of the wave function of interest when crossing the common boundary between two neighboring elements, one introduces so-called "bridge" functions. Except for these bridge functions, which connect the two elements, all DVR basis functions are nonzero only within their respective element. Note that derivative continuity is neither theoretically required nor important in practice. This leads to an optimal spatial representation for the time-propagation step, especially when developing a parallel implementation where communication between processors needs to be minimized. For a given set of finite elements and mesh points, the relevant globally normalized DVR basis $\{f_i(r)\}$ can be uniquely determined. More details were given by Rescigno and McCurdy [21]. In this work, we also use the Gauss-Lobatto mesh points for all elements. However, we remove the first and last DVR functions to explicitly account for the boundary conditions.

We further expand the wave functions of the helium atom in singlet (total spin $S=0$) or triplet ($S=1$) spin states as

$$\Psi^S(\boldsymbol{r}_1,\boldsymbol{r}_2,t) = \sum_{Ll_1l_2}\sum_{j<i}\Big[f_i(r_1)f_j(r_2)C^{ij}_{l_1l_2L}(t) + (-1)^{\delta} \times f_j(r_1)f_i(r_2)C^{ij}_{l_2l_1L}(t)\Big]\mathcal{Y}^{LM}_{l_1l_2}(\Omega_1,\Omega_2) + \sum_{Ll_1\le l_2}\sum_i f_i(r_1)f_i(r_2)C^{ii}_{l_1l_2L}(t)\frac{1}{1+\delta_{l_1l_2}} \times\Big[\mathcal{Y}^{LM}_{l_1l_2}(\Omega_1,\Omega_2) + (-1)^{\delta}\mathcal{Y}^{LM}_{l_2l_1}(\Omega_1,\Omega_2)\Big]. \quad (1)$$

Here we defined the phase factor $\delta \equiv l_1+l_2-L+S$. The unknown coefficients $C^{ij}_{l_1l_2L}(t)$ explicitly depend on the time $t$ if the helium atom is subjected to a time-dependent external field. In the above representation, we notice that $\Psi^S(\boldsymbol{r}_2,\boldsymbol{r}_1,t)=(-1)^S\Psi^S(\boldsymbol{r}_1,\boldsymbol{r}_2,t)$ under exchange of the two electrons. Since our initial (ground) state is a singlet state, we will only consider the $S=0$ case below. The summation over $(l_1l_2)$ includes all possible combinations of $l_1$ and $l_2$ forming the total angular momentum $L$ and a given parity $\pi$. For example, if $l_1 \neq l_2$, we need to include the partial wave $(l_1,l_2)$ as well as $(l_2,l_1)$. On the grid points, the DVR basis functions in Eq. (1) satisfy $f_i(r_j)=\delta_{ij}/\sqrt{\omega_i}$, where $\omega_i$ is a weight factor determined by the particular DVR scheme (here Gauss-Lobatto). If the laser pulse is polarized along the $z$ axis, the total angular magnetic quantum number $M$ is conserved. Hereafter, we assume $M=0$ for such a linearly polarized pulse without loss of generality. As a consequence, we are left with a five-dimensional problem characterized by the angular momenta $\{Ll_1l_2\}$ and the radial mesh points $\{r_i,r_j\}$.

It is worthwhile to make a few comments regarding the set of time-dependent expansion coefficients $\{C^{ij}_{l_1l_2L}(t)\}$. First, it is important to realize that we must have

$$C^{ii}_{l_1 l_2 L}(t) = C^{ii}_{l_2 l_1 L}(t) \tag{2}$$

for the singlet state and

$$C^{ii}_{l_1 l_2 L}(t) = 0 \tag{3}$$

for the triplet state. Along the diagonal line, where $r_j = r_i$, $C^{ii}_{l_1 l_2 L}(t)$, and $C^{ii}_{l_2 l_1 L}(t)$ for a pair of partial waves are thus not independent of each other. They must satisfy Eq. (2) for our case of interest. On the other hand, we would not need to use the mesh points at the line $r_j = r_i$ to discretize the triplet states because of Eq. (3). Therefore, the second summation term in Eq. (1) can be dropped.

Second, a closer look at the coefficients reveals that

$$C^{ij}_{l_1 l_2 L}(t) = (\omega_i \omega_j)^{1/2} \langle \mathcal{Y}^{LM}_{l_1 l_2}(\Omega_1, \Omega_2) | \Psi(\boldsymbol{r}_1, \boldsymbol{r}_2, t) |^{r_1 = r_i}_{r_2 = r_j}. \tag{4}$$

As expected, the expansion coefficient $C^{ij}_{l_1 l_2 L}(t)$ is just the value of the radial function on the mesh point $(i,j)$, multiplied by weight factors for the Gaussian integration. Finally, we stress that, in the present representation, only mesh points in the lower triangular region are built into the wave function, i.e., indices $j \leq i$ in Eq. (1). The values of the wave function in the upper triangular region $(r_2 \geq r_1)$ can be determined uniquely by using the exchange symmetry of the system.

All the one-electron Hamiltonian and dipole matrices are set up on the mesh points we discussed above. An issue worth emphasizing concerns the calculation of the matrix elements of the two-electron Coulomb repulsion interaction $1/|\boldsymbol{r}_1 - \boldsymbol{r}_2|$ in the present FE-DVR scheme. In the multipole expansion, $V^{\lambda}(r_1, r_2) = r^{\lambda}_{<}/r^{\lambda+1}_{>}$ has a cusp at $r_1 = r_2$, which leads to a discontinuity in the first-order derivative. It therefore might be a poor description if the matrix elements are approximated by $V^{\lambda}_{ij,i'j'} = \delta_{ii'}\delta_{jj'} r^{\lambda}_j / r^{\lambda+1}_i$. Here, we follow the idea of McCurdy *et al.* [22,23] to calculate the matrix elements by solving a Poisson equation. By doing so, all the matrix elements of the potential remain diagonal with respect to the radial coordinates as well, without loss of accuracy.

In the length gauge, the resulting time-dependent Schrödinger equation for the helium atom in a linearly polarized laser pulse can be written as

$$\mathrm{i}\frac{\partial}{\partial t} C^{ij}_{l_1 l_2 L}(t) = \sum_{j' \leq i'} \sum_{\{l'_1 l'_2 L'\}} [H^{i'j'l'_1 l'_2 L'}_{ijl_1 l_2 L} + E_0 f(t) \sin(\omega t) \times (z_1 + z_2)^{i'j'l'_1 l'_2 L'}_{ijl_1 l_2 L}] C^{i'j'}_{l'_1 l'_2 L'}(t), \tag{5}$$

where $H^{i'j'l'_1 l'_2 L'}_{ijl_1 l_2 L}$ are the matrix elements of the field-free Hamiltonian. Furthermore, $E_0$ and $\omega$ denote the peak strength of the electric field and the photon angular frequency (i.e., the photon energy in atomic units), respectively, while $f(t)$ describes the time-dependent envelope of the applied laser pulse. In Eq. (5), the summations over $j' \leq i'$ and $\{l'_1 l'_2 L'\}$ mean that the sums are running over all possible partial waves if $j' < i'$ but only include partial waves with $l'_1 \leq l'_2$ if $j' = i'$. Note that using the FE-DVR scheme allows us to represent the Hamiltonian as an extremely sparse matrix, whose nonzero elements are concentrated along the diagonal.

In the present work, the solution for the time-dependent coefficients $\{C^{ij}_{l_1 l_2 L}(t)\}$ is achieved via a high-order Arnoldi-Lanczos algorithm. Denoting $\boldsymbol{C}(t)$ as the vector containing all the coefficients $C^{ij}_{l_1 l_2 L}(t)$, we determine $\boldsymbol{C}(t+\Delta t) = \exp[-\mathrm{i}H(t)\Delta t]\boldsymbol{C}(t)$ for a sufficiently small time step $\Delta t$. A significant advantage of this time evolution scheme is the fact that only matrix-vector multiplications are required. These, in turn, benefit from the sparse matrices involved in the FE-DVR approach. We refer the readers to Ref. [24] for more details and discussions regarding the application of the Arnoldi-Lanczos algorithm to solving the TDSE.

During the time evolution, the time-dependent values of the radial wave function of the two-electron system on the $(r_1, r_2)$ grid can be directly obtained without ever resorting to one-electron orbitals. This provides an excellent representation of the *combined* response by the laser-driven correlated system. It is another one of the appealing features in the present application of the FE-DVR scheme to the problem of double photoionization.

### B. Initial state of the helium atom

Due to the large size of the Hamiltonian matrix, it is entirely impractical (and unnecessary) to directly diagonalize the Hamiltonian to obtain the initial ground state. In this work, we set $\Delta t \to -\mathrm{i}\Delta t$ and relax the system from an arbitrary spatial distribution to obtain the wave function of the ground state. Time evolution in imaginary time is again achieved by means of the Arnoldi-Lanczos algorithm. For a sufficiently long propagation time, the system settles down into its lowest eigenstate. Specifically, we use

$$E = -\frac{1}{2\Delta t} \lim_{t \to +\infty} \ln \left\{ \frac{\langle \Psi(t+\Delta t) | \Psi(t+\Delta t) \rangle}{\langle \Psi(t) | \Psi(t) \rangle} \right\}. \tag{6}$$

In the present work, we use a spatial box of $r_{\max} = 60$ a.u., divided into 150 finite elements with four Gauss-Lobatto DVR basis functions set up in each element. Using angular momenta $l_{1,2} \leq 3$, the ground-state energy was obtained as $-2.903041$ a.u., which is sufficiently accurate for the present purpose.

### C. Extraction of the cross sections in two-photon double ionization process

We now discuss the extraction of the total (neither the energies nor the angles are resolved) and the fully differential (energies and angles resolved) for double photoionization. As commented upon earlier, there are not only discrepancies between calculations that include electron correlation in the final state, but there are also differences between calculations that use uncorrelated final-state wave functions to extract the cross sections. For example, Foumouo *et al.* [12] obtain very different results with or without accounting for the full long-range correlation between all three charged particles in the final state. Horner *et al.* [14], on the other hand, claim to also have included this interaction in a sufficiently accurate way through exterior complex scaling. Their expression to com-

pute the required projection coefficient is based on a surface integral involving an uncorrelated final state and the derivative of the exact scattering wave function. Finally, Ivanov and Kheifets [13] project to a field-free momentum-space convergent close-coupling wave function, which also contains correlation effects to large distances. Both of the latter sets of results [13,14], are similar to those obtained in several other approaches, where the cross section was extracted by projecting to an uncorrelated product of two Coulomb waves. However, there are still discrepancies of about a factor of 2 among the results obtained in a number of these calculations.

In an attempt to clarify the situation, it seems reasonable to first determine numerically reliable results for the various cross sections by neglecting the electron-electron interaction in the projection state before addressing the much more complicated three-body breakup problem in a fully correlated way. Since the former has not yet been achieved in a satisfactory manner, due to reasons unrelated to correlations in the projection state (see below), we follow the example of previous works and construct the field-free two-electron double continuum state as an uncorrelated product of one-electron continuum states.

For a one-electron system, we have

$$\Phi_{\boldsymbol{k}}^{(-)}(\boldsymbol{r}) = \frac{1}{k}\sum_{lm} \mathrm{i}^{l} e^{-\mathrm{i}\sigma_l(k)} \varphi_{kl}^{(c)}(r) Y_{lm}(\hat{\boldsymbol{r}}) Y_{lm}^{*}(\hat{\boldsymbol{k}}), \tag{7}$$

with the asymptotic behavior

$$\varphi_{kl}^{(c)}(r) \underset{r\to\infty}{\sim} \sqrt{\frac{2}{\pi}} \sin\left(kr + \frac{Z}{k}\ln 2kr - \frac{l\pi}{2} + \sigma_l\right), \tag{8}$$

where $\sigma_l$ denotes the Coulomb phase. The radial continuum wave function satisfies

$$\int_0^{+\infty} \varphi_{kl}^{(c)}(r)\varphi_{k'l}^{(c)}(r)dr = \delta(k-k'). \tag{9}$$

Thus, our continuum states are normalized in momentum space according to $\langle \Phi_{\boldsymbol{k}}^{(-)} | \Phi_{\boldsymbol{k}'}^{(-)} \rangle = \delta(\boldsymbol{k}-\boldsymbol{k}')$.

The singlet two-electron continuum wave function satisfying the incoming boundary condition (−) is given by

$$\Psi_{\boldsymbol{k}_1,\boldsymbol{k}_2}^{(-)}(\boldsymbol{r}_1,\boldsymbol{r}_2) = \frac{1}{\sqrt{2}}[\Phi_{\boldsymbol{k}_1}^{(-)}(\boldsymbol{r}_1)\Phi_{\boldsymbol{k}_2}^{(-)}(\boldsymbol{r}_2) + \Phi_{\boldsymbol{k}_2}^{(-)}(\boldsymbol{r}_1)\Phi_{\boldsymbol{k}_1}^{(-)}(\boldsymbol{r}_2)]. \tag{10}$$

It is normalized in momentum space according to

$$\langle \Psi_{\boldsymbol{k}_1,\boldsymbol{k}_2}^{(-)} | \Psi_{\boldsymbol{k}_1',\boldsymbol{k}_2'}^{(-)} \rangle = \delta(\boldsymbol{k}_1-\boldsymbol{k}_1')\delta(\mathbf{k}_2-\boldsymbol{k}_2') + \delta(\boldsymbol{k}_1-\boldsymbol{k}_2')\delta(\boldsymbol{k}_2-\boldsymbol{k}_1'). \tag{11}$$

In the present work, the discretized Coulomb continuum state $\varphi_{kl}^{(c)}(r)$ is obtained by solving the one-electron Schrödinger equation for the $He^+$ ion ($Z=2$), using the same mesh points as for the neutral helium atom. This yields a self-consistent grid representation of the time-evolved wave packet and the final continuum states. Care must be taken regarding mesh points on the edge of the spatial box, where the continuum states generally have a nonvanishing probability distribution. A matching procedure using the asymptotic behavior of the Coulomb continuum wave function was employed to renormalize the numerical solutions in momentum space. Checking our results against those from the routine COULFG of Barnett [25] showed excellent agreement.

In practice, there are two approaches to produce the Coulomb wave function in the DVR scheme. The strategy discussed above is one in which the box size is fixed. Another one is to directly diagonalize the Hamiltonian matrix while satisfying bound-state boundary conditions. A continuum state with any desired positive energy can then be found by varying the size of the box. An advantage of this approach is the straightforward way to renormalize the wave function to the energy space through multiplication by $\rho^{1/2}(E_i)$, where $\rho(E_i)$ is the density of states at the energy $E_i$. Our numerical experiments, however, showed that the latter method is more time consuming than the former.

Note that the final double-continuum state, when approximated by a product of two Coulomb waves with $Z=2$, is orthogonal to the single-continuum channels, which themselves are approximated as a product of a bound hydrogenic $1s$ orbital ($Z=2$) and a Coulomb wave for $Z=1$. Within these approximations, therefore, no interference between single-continuum and double-continuum channels needs to be considered, due to the removal of the contributions from the single-ionization channels.

Therefore, after subtracting the overlap with the initial bound state, the probability amplitude for the two-photon double ionization at the end of the laser pulse can be written as

$$\langle \Psi_{\boldsymbol{k}_1,\boldsymbol{k}_2}^{(-)} | \Psi(t) \rangle = \sum_{L=0,2}\sum_{l_1 l_2} (-\mathrm{i})^{l_1+l_2} e^{\mathrm{i}[\sigma_{l_1}(k_1)+\sigma_{l_2}(k_2)]} \times \mathcal{Y}_{l_1 l_2}^{LM}(\hat{\boldsymbol{k}}_1,\hat{\boldsymbol{k}}_2)\mathcal{F}_{l_1 l_2}^{L}(k_1,k_2). \tag{12}$$

The partial-wave amplitude in momentum space satisfies the exchange symmetry

$$\mathcal{F}_{l_2 l_1}^{L}(k_2,k_1) = (-1)^{\delta}\mathcal{F}_{l_1 l_2}^{L}(k_1,k_2). \tag{13}$$

Physically, the quantity $\langle \Psi_{\boldsymbol{k}_1,\boldsymbol{k}_2}^{(-)} | \Psi(t) \rangle$ corresponds to the probability amplitude for two electrons escaping with momenta $k_1$ and $k_2$ in the directions of $\hat{\boldsymbol{k}}_1$ and $\hat{\boldsymbol{k}}_2$ after absorbing the photons. The total cross section for the nonsequential (NS) two-photon DI is given by

$$\sigma_{\mathrm{NS}} = \left(\frac{\omega}{I_0}\right)^2 \frac{\mathcal{P}_{kk}}{T_{\mathrm{eff}}^{(2)}}, \tag{14}$$

where $I_0$ is the peak intensity, $\mathcal{P}_{kk}$ denotes the probability for double ionization, and $T_{\mathrm{eff}}^{(2)}$ is an "effective interaction time." These will be further discussed below.

For time-dependent calculations, a few words about the validity of Eq. (14) are necessary. First of all, the formula for the generalized cross section $\sigma_{\mathrm{NS}}$ given in Eq. (14) is *only valid for the direct or nonsequential process*, in which the ionization probability is proportional to the pulse duration. On the other hand, if two electrons are kicked out in a sequential way, the ionization probability is proportional to the square of the pulse duration rather than the pulse duration

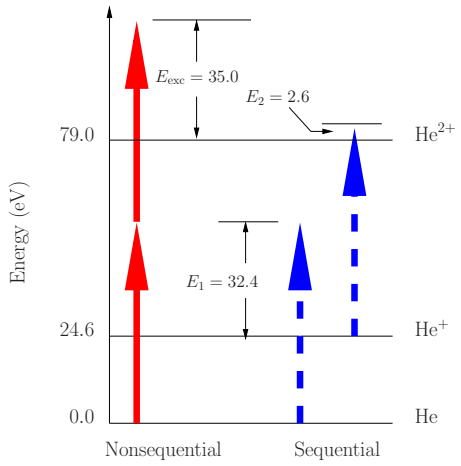


FIG. 1. (Color online) Schematic representation of the helium energy levels involved in the double ionization by absorption of two photons for a photon energy of 57 eV. The energies are given in units of eV in the diagram. The nonsequential and sequential ionization mechanisms are represented by the solid and dashed arrows, respectively.

itself. This can occur, and usually does, for $\omega > 54.4$ eV in helium. The two photons are then predominantly absorbed one after the other, almost independently of each other. The two possibilities are depicted in Fig. 1 for a photon energy of 57 eV, where both sequential and nonsequential channels are open. In this case, it is not straightforward to define either the ionization rate or the cross section for the entire event.

Furthermore, we have to ensure that the system irradiated by the intense xuv pulse is far from saturation. This requires that a laser pulse of relatively low intensity and short interaction time must be employed in numerical calculations. An effective interaction time $T_{\text{eff}}^{(N)}$ for an $N$-photon process is then defined by [12]

$$T_{\text{eff}}^{(N)} \equiv \int_0^\tau f^{2N}(t)dt, \tag{15}$$

with the result

$$T_{\text{eff}}^{(2)} = 35\tau/128 \tag{16}$$

for a sine-squared pulse shape of a duration of $\tau$.

On the other hand, we need to propagate the system on a relatively long time scale to extract the cross-section information. As a consequence, the laser parameters must be chosen in a properly balanced way for practical calculations. For the present case of interest, peak intensities between $10^{14}$ and $10^{15}$ W/cm$^2$ and time durations of 10–15 optical cycles meet the above criteria.

In a time-dependent formulation, therefore, the dependence of the $N$-photon cross section on the number of photons absorbed not only occurs through the factor $(\omega/I_0)^N$, but also through the effective interaction time defined above. As seen from the definition, the result depends explicitly on how many photons are being absorbed.

The energy sharing between the two escaping electrons can be uniquely determined through the hyperangle $\alpha = \tan^{-1}(k_2/k_1)$. We set $E_1 = E_{\text{exc}} \cos^2 \alpha$ and $E_2 = E_{\text{exc}} \sin^2 \alpha$, where $E_{\text{exc}} = 2\omega - I^{2+}$ is the excess energy for two-photon double ionization. For a given energy sharing $\alpha$, the triple-differential cross section (TDCS) can be written as

$$\frac{d^3\sigma}{d\alpha\, d\hat{\mathbf{k}}_1\, d\hat{\mathbf{k}}_2} = \left(\frac{\omega}{I_0}\right)^2 \frac{1}{T_{\text{eff}}^{(2)}} \int\int dk_1'\, dk_2'\, k_1'^2 k_2'^2 \times \delta\left(\alpha - \tan^{-1}\left(\frac{k_2'}{k_1'}\right)\right) |\langle \Psi_{\mathbf{k}_1',\mathbf{k}_2'}^{(-)} | \Psi(t) \rangle|^2. \tag{17}$$

It is important to remember that there are two indistinguishable electrons in the final channel, and hence the energy sharings described by $\alpha$ and $\pi/2 - \alpha$ represent the same observable event. Therefore, we either need to consider $0 \le \alpha \le \pi/4$ or $\pi/4 \le \alpha \le \pi/2$ to avoid double counting. The TDCS with respect to the energy of one electron is then given by

$$\frac{d^3\sigma}{dE_1\, d\hat{\mathbf{k}}_1\, d\hat{\mathbf{k}}_2} = \frac{1}{k_1 k_2 \cos^2 \alpha} \left(\frac{\omega}{I_0}\right)^2 \frac{1}{T_{\text{eff}}^{(2)}} \times \int\int dk_1'\, dk_2'\, k_1' \delta(k_2' - k_1' \tan \alpha) \times \left| \sum_{L=0,2,l_1 l_2} \chi_{l_1 l_2}(k_1', k_2') \mathcal{Y}_{l_1 l_2}^{LM}(\hat{\mathbf{k}}_1, \hat{\mathbf{k}}_2) \mathcal{F}_{l_1 l_2}^{L}(k_1', k_2') \right|^2, \tag{18}$$

where we have defined the phase factor

$$\chi_{l_1 l_2}(k_1, k_2) = (-\mathrm{i})^{l_1 + l_2} e^{\mathrm{i}[\sigma_{l_1}(k_1) + \sigma_{l_2}(k_2)]}. \tag{19}$$

By collecting all ionization events, the total cross section for two-photon double ionization is then given by

$$\sigma_{\text{NS}} = \int d\alpha \int d\hat{\mathbf{k}}_1\, d\hat{\mathbf{k}}_2 \frac{d^3\sigma}{d\alpha\, d\hat{\mathbf{k}}_1\, d\hat{\mathbf{k}}_2} = \left(\frac{\omega}{I_0}\right)^2 \frac{1}{T_{\text{eff}}^{(2)}} \int\int dk_1\, dk_2 \frac{d^2\mathcal{P}(k_1, k_2)}{dk_1\, dk_2}. \tag{20}$$

Here we have introduced the momentum distribution

$$\frac{d^2\mathcal{P}(k_1, k_2)}{dk_1\, dk_2} = \sum_{L=0,2} \sum_{l_1 l_2} |\mathcal{F}_{l_1 l_2}^{L}(k_1, k_2)|^2. \tag{21}$$

Similarly, the corresponding two-electron energy distribution is given by

$$\frac{d^2\mathcal{E}(E_1, E_2)}{dE_1\, dE_2} = \frac{1}{k_1 k_2} \frac{d^2\mathcal{P}(k_1, k_2)}{dk_1\, dk_2}. \tag{22}$$

Due to the limited pulse duration and thus a finite laser bandwidth, the energies of the two escaping electrons generally do not satisfy the condition of $E_1 + E_2 = E_{\text{exc}}$ exactly. This is the principal reason to introduce momentum or energy distributions, which are spread out but peak around the above result. Details about how the two escaping electrons gain

their kinetic energy can be understood by monitoring the energy distribution during the interaction with the applied pulse.

## III. RESULTS AND DISCUSSION

As mentioned previously, we confine the system to a spatial box of $r_{max}=60$ a.u. This truncated configuration space is further divided into 150 finite elements, with four Gauss-Lobatto DVR basis functions set up in each element. The distribution of the elements is chosen in such a way that the spatial variation of the wave function close to the nucleus (determined by the nuclear charge $Z$) and far away from the nucleus (determined by the highest energy of a free electron) can be represented accurately. We also checked that the results presented below do not change within the thickness of the line when the box size is enlarged to $r_{max}=80$ a.u.

Having obtained the initial state of the system as described above, the time propagation in the laser field is accomplished through the Arnoldi-Lanczos algorithm. Compared to other time-propagation approaches, such as leapfrog or a split-operator approach [9], the present scheme allows us to take relatively large steps in time. Specifically, using only 400 steps per optical cycle is sufficient to achieve converged solutions of the TDSE for the cases presented in this paper. Most of the results presented below were obtained with a sine-squared pulse with a peak intensity of either $5\times10^{14}$ or $3\times10^{15}$ W/cm$^2$ and a time duration of ten optical cycles. However, we will also discuss the dependence of the results on the length of the pulse.

Figure 2 shows our results for the radial electron density after five and ten optical cycles of a 42 eV laser pulse with a duration of ten optical cycles, a sine-squared envelope, and a peak intensity of $5\times10^{14}$ W/cm$^2$. The high densities near the edges correspond to excitation and single ionization, while double ionization corresponds to the regime where both $r_1$ and $r_2$ are large. The lack of structure in this regime indicates that the double ionization occurs in a nonsequential manner, leading to a smooth distribution.

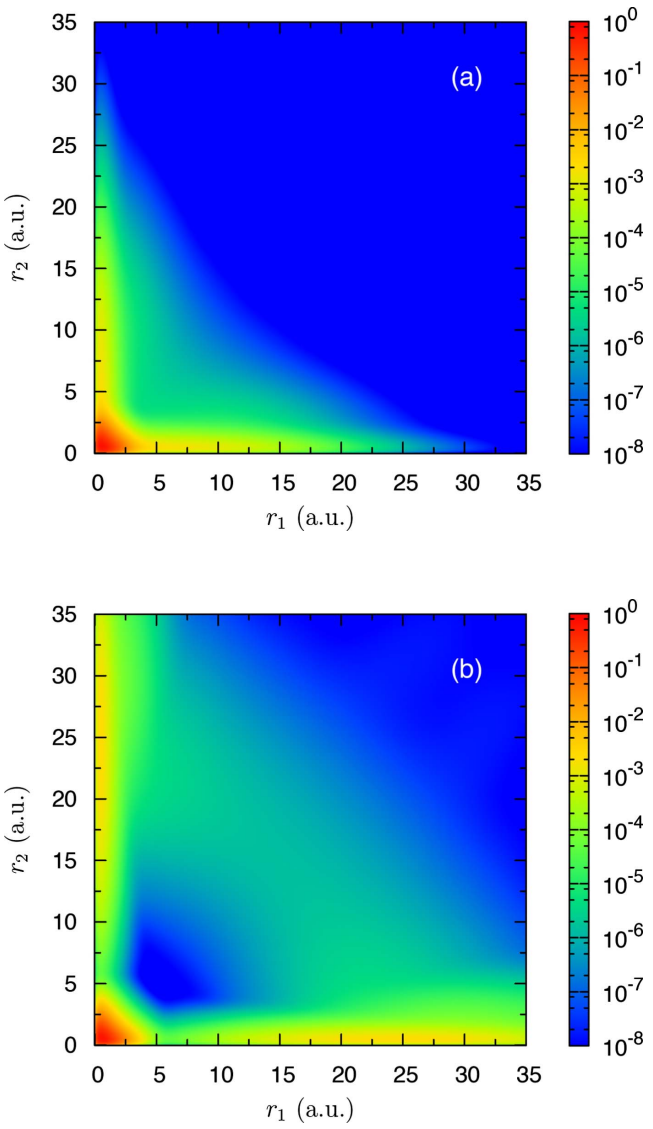


FIG. 2. (Color online) Radial electron density after five (a) and ten (b) optical cycles of a 42 eV laser pulse with a duration of ten optical cycles, a sine-squared envelope, and a peak intensity of $5\times10^{14}$ W/cm$^2$.

### A. Angle-integrated cross section

Figure 3 shows our results for the total two-photon double-ionization cross section of He over a range of photon energies from threshold to 54 eV, i.e., just below the energy where sequential double ionization becomes possible. These results are compared with a number of recently published theoretical predictions and also with an experimental measurement for the incident photon energy of 41.8 eV by Hasegawa *et al.* [16]. The results are presented on both a logarithmic and a linear scale, with the latter being more appropriate to discuss the similarities and remaining differences between some of the very close predictions.

To begin with, we notice excellent agreement between our predictions and those obtained by Laulan and Bachau [10] as well as Foumouo *et al.* [12] in their "no correlation" (NC) model, i.e., where the uncorrelated product of the two Coulomb functions is used to extract the cross section from the propagated wave function. There is also satisfactory, though not perfect agreement with the published results of Feng and van der Hart [11], who used an effectively time-independent $R$-matrix-Floquet method and those of Ivanov and Kheifets [13], who used the convergent close-coupling method to generate the field-free two-electron continuum wave function, on which the time-propagated wave function was projected. Very close agreement is also obtained with the results of Hu *et al.* [9], provided we multiply their published result by $128/70\approx1.83$. This modification of the Hu *et al.* results is appropriate, since they simply used $\tau/2$ for the effective interaction time $T_{\mathrm{eff}}^{(2)}$. Hence, the discrepancy between the published results of Hu*et al.* [9] and many of the other calculations using the same uncorrelated state for projection seems to be due entirely to the factor $T_{\mathrm{eff}}^{(2)}$ rather than to an originally suspected pulse-shape and/or peak-intensity dependence of the results. Questions of intensity dependence, or the lack thereof, will be further discussed below. Finally, we

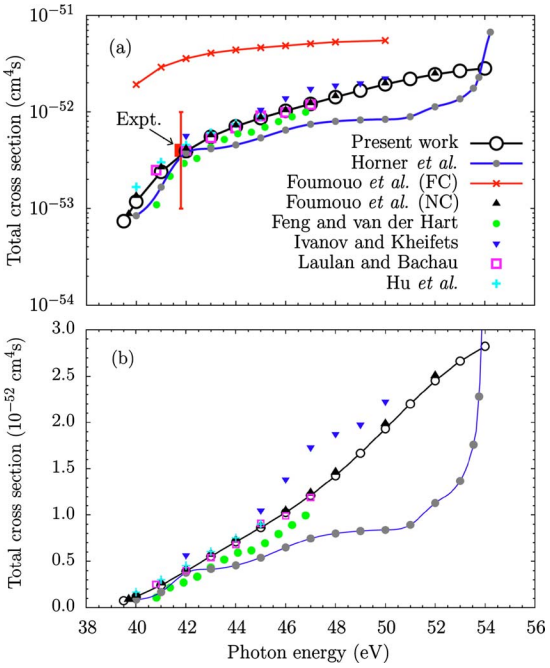


FIG. 3. (Color online) Total angle-integrated cross section for two-photon double ionization of helium as a function of the photon energy on both a logarithmic (a) and linear (b) scale. The various theoretical approaches are described in the text. Note that the published results of Hu *et al.* [9] were multiplied by a factor of 128/70. A laser pulse with a duration of ten optical cycles, a sine-squared envelope, and a peak intensity of $5\times10^{14}$ W/cm$^2$ was used in the present calculations.

are aware of another ongoing effort by Feist *et al.* [26], who use a similar approach to ours with a different and entirely independent numerical implementation. Not surprisingly, we have been informed [27] that their results (not shown) are very close to ours.

There are two other sets of predictions shown in Fig. 3, namely, those obtained by Foumouo *et al.* [12] in their "full correlation" (FC) model, in which the time-propagated wave function was projected to correlated field-free close-coupling-type wave function generated by the *J*-matrix method, and recent results by Horner *et al.* [14] obtained using a time-independent exterior complex scaling method. Both of these sets of predictions differ significantly from the others, with the FC results being nearly an order of magnitude larger in the near-threshold regime. This is very surprising, since the two-electron continuum wave function was generated in a similar way to the CCC approach, i.e., one of the electrons is described by a true continuum orbital while the other is represented by a square-integrable pseudostate. Hence one might expect similar results from the two approaches. Note that Horner *et al.* [14] also claim to have accounted for electron correlations to essentially the full extent, but their results are generally the smallest of all sets. Except for the FC results, and those of Nikolopoulos and Lambropoulos [28,29] (not shown, since they are even higher than the FC values), all theoretical predictions, including the latest set of Shakeshaft [15] (not shown), are compatible with the only existing experimental data point of

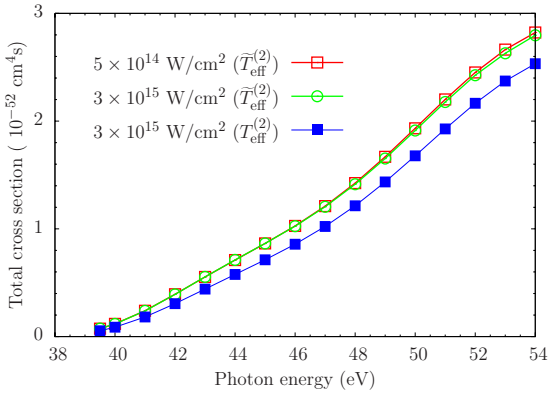


FIG. 4. (Color online) Total cross section of the two-photon double ionization of the helium atom, as obtained for a sine-squared 42 eV laser pulse of ten optical cycles with peak intensities of $5\times10^{14}$ and $3\times10^{15}$ W/cm$^2$. The results shown for an effective interaction time $\tilde{T}^{(2)}_{\rm eff}$ account for the depletion of the ground-state population (see the text).

Hasegawa *et al.* [16], which has an approximate uncertainty of one order of magnitude according to the authors [30].

We are not in a position to comment or speculate on possible reasons for the remaining discrepancies, but the current work, and that of Feist *et al.* [26], have already motivated additional calculations, for example, by Horner [31]. Hopefully, this work will either remove or shed more light on the origin of the remaining discrepancies. It seems clear, however, that there are now several highly accurate numerical models available, which have been implemented independently by several groups, and which yield the same results for the well-defined NC theoretical model in the perturbative regime. These methods predict a smooth, almost linear increase of the two-photon double-ionization cross section for He in its ground state between the thresholds for nonsequential (39.5 eV) and sequential ionization (54.4 eV). A closer look at some of the predictions reveals fluctuations that seem to be of numerical rather than of physical nature.

Next, we turn to a potential dependence of the extracted cross section on the peak intensity of the applied laser field.

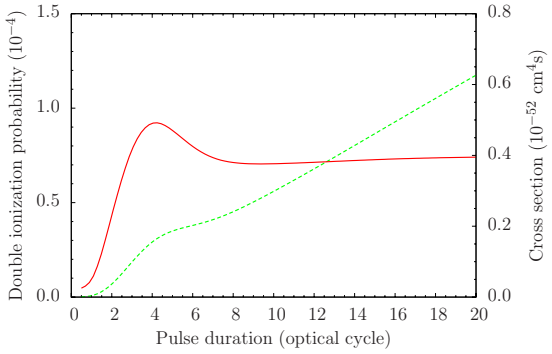


FIG. 5. (Color online) Total probability (dashed line, left scale) for two-photon double ionization and the corresponding generalized total cross section (solid line, right scale) for the two-photon double ionization of helium, as obtained for a 42 eV laser pulse with a sine-squared envelope and a peak intensity of $5\times10^{14}$ W/cm$^2$ for pulse lengths varying between 0 and 20 optical cycles.

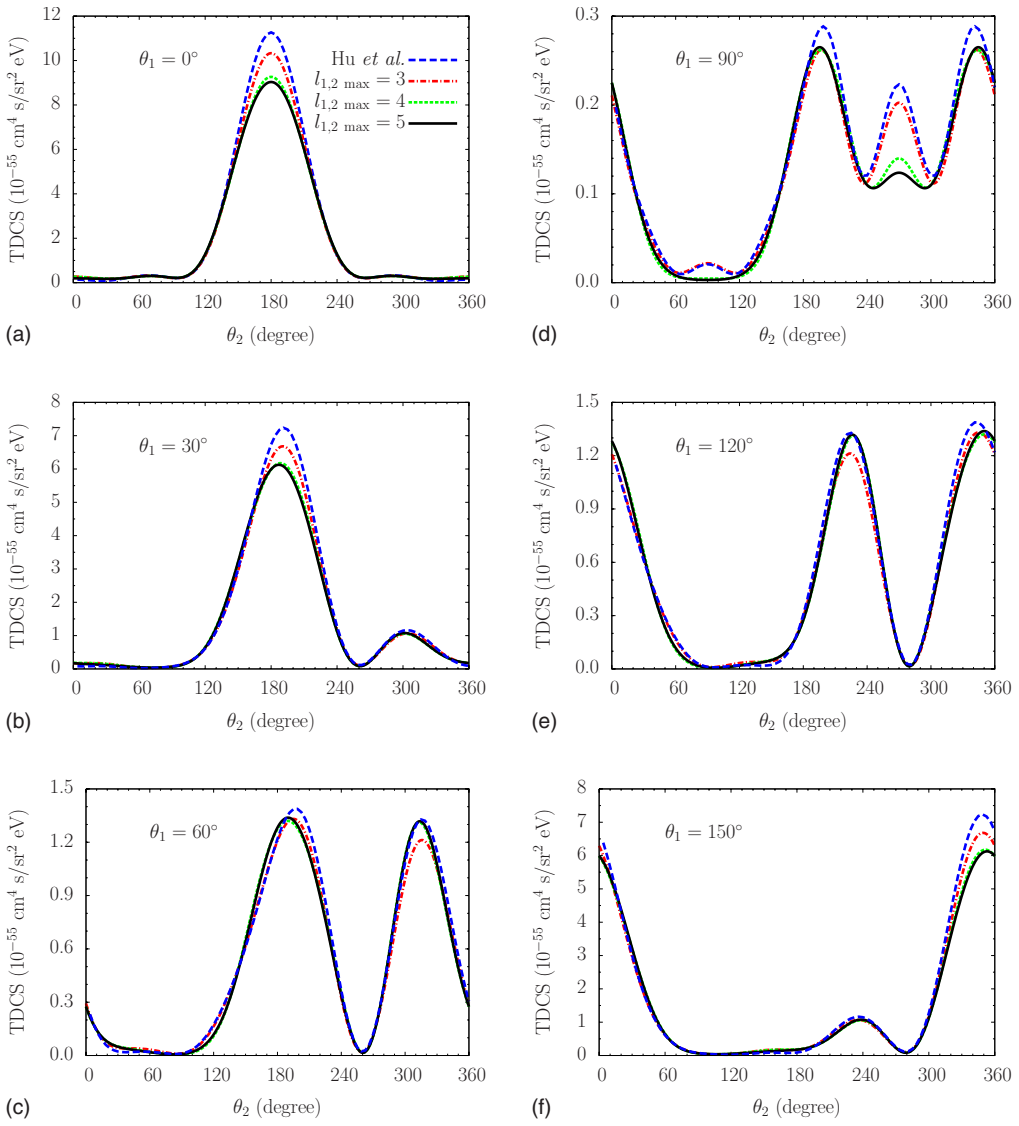


FIG. 6. (Color online) The coplanar triple-differential cross section for two-photon DI of helium in a ten-cycle sine-squared laser pulse of central photon energy 42 eV and peak intensity $5\times10^{14}$ W/cm$^2$ for equal energy sharing ($E_1=E_2=2.5$ eV) of the two outgoing electrons. The angle listed in the figure is the angle between the laser polarization vector and one of the two escaping electrons, while the emission angle of the second electron varies. Our results for $(L_{\max},l_{1,\max},l_{2,\max})=(3,3,3)$, (3,4,4), and (3,5,5) are compared with the (3,3,3) results of Hu *et al.* [9] after multiplication of the latter results by 128/70.

As mentioned above, such a dependence was originally proposed by Hu *et al.* [9] to explain the differences between their results and those of Piraux *et al.* [32], which are essentially the same as the NC results of Foumouo *et al.* [12]. We will now show that such an intensity dependence does not exist, at least not for the intensities considered here, if the depopulation of the initial state is properly accounted for.

At the end of the laser pulse we have

$$\mathcal{P}_{kk} = \sigma_{\rm NS}\int_0^\tau F^2(t)\mathcal{P}_{\rm gs}(t)dt \tag{23}$$

for the direct two-photon double ionization. Here $\mathcal{P}_{\rm gs}(t)$ is the survival probability of the initial state in the time-dependent laser field and

$$F(t) = \frac{I_0}{\omega}f^2(t) \tag{24}$$

is the photon flux. For a relatively weak peak intensity and a short time duration of the pulse, the system is only weakly ionized and we may use the approximation $\mathcal{P}_{\rm gs}(t)\simeq 1$. Independent of the laser intensity, this yields an effective time of $35\tau/128$ for a $\sin^2$ pulse of total length $\tau$. In order to ensure the validity of the above approximation, Foumouo *et al.* [12] used a peak intensity of only $10^{13}$ W/cm$^2$ and a pulse duration of ten optical cycles. Due to the small ponderomotive energy and the large photon energy, on the other hand, lowest nonvanishing order of perturbation theory is actually expected to be still valid for the two-photon double-ionization process at much higher peak intensities, at least up to about $10^{15}$ W/cm$^2$. The introduction of a cross-section concept

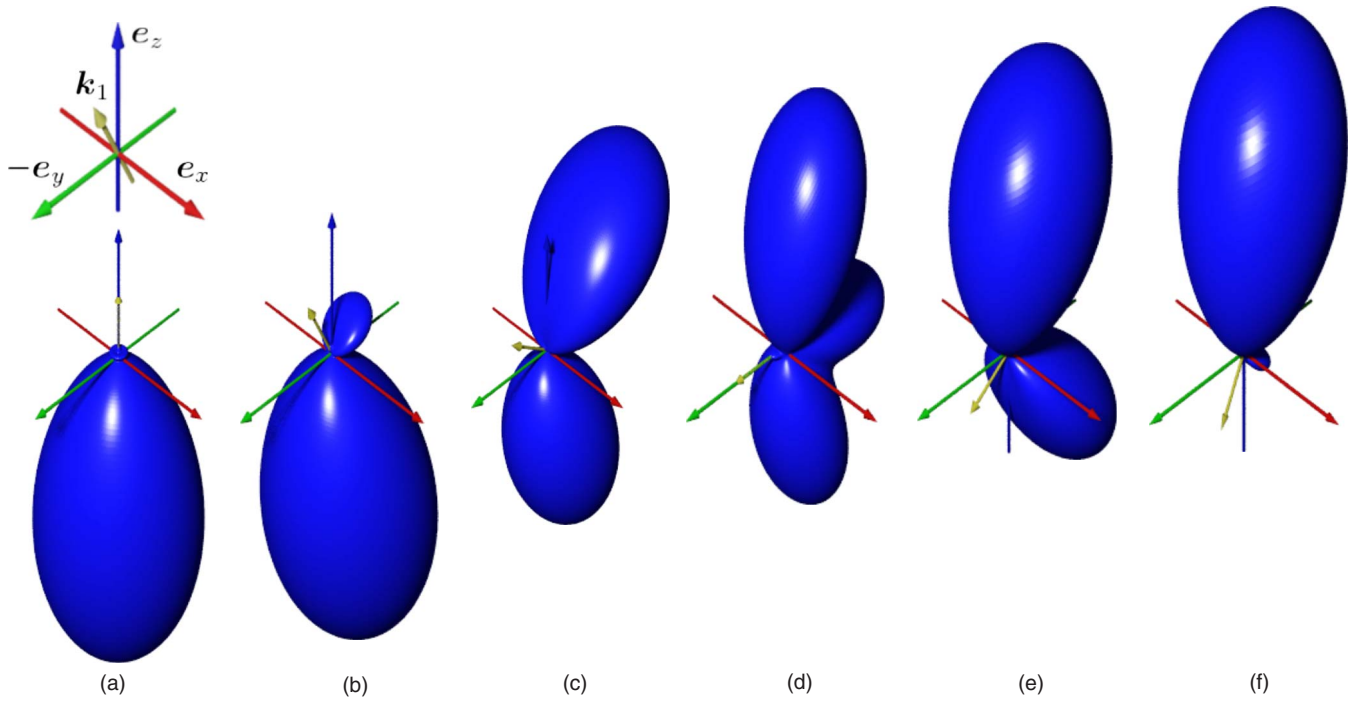


FIG. 7. (Color online) The TDCS in 3D representation. The laser parameters are the same as in Fig. 6. The polarization vector of the laser light ($z$ axis) and the emission angle of one of the escaping electrons ($\hat{\boldsymbol{k}}_1$) define the $yz$ plane. The results are for angles of 0° (a), 30° (b), 60° (c), 90° (d), 120° (e), and 150° (f) between $\hat{\boldsymbol{k}}_1$ and the $z$ axis. Because of the dependence of the magnitudes on $\hat{\boldsymbol{k}}_1$ (see also Fig. 6), each figure has been individually scaled.

would make little sense if the result were strongly affected by the field intensity itself.

Consequently, one should address the following questions: (1) How do the approximations above behave if the peak intensity is boosted, for example, to $10^{15}$ W/cm$^2$ or even higher? (2) Is the concept and the subsequent calculation of cross sections still meaningful at such high intensities?

We will now attempt to answer these questions by taking a closer look at the survival probability of the ground state. For a photon energy of 42 eV, a peak intensity of $5\times10^{14}$ W/cm$^2$ for the sine-squared pulse, and a pulse duration of ten optical cycles, we find $\mathcal{P}_{\text{g.s.}}=0.922$ at the end of the pulse. Hence, the approximation $\mathcal{P}_{\text{g.s.}}(t)\simeq 1$ is still accurate within a few percent. For the same pulse parameters, except for a peak intensity of $3\times10^{15}$ W/cm$^2$, on the other hand, we obtain a survival probability of only 0.615 at the end of the pulse. Hence, if we still want to use the same method, we need to account for this depopulation of the initial state. Since $\mathcal{P}_{\text{g.s.}}(t)\leq 1$ at all times, one should use the definition

$$\tilde{T}^{(2)}_{\text{eff}} \equiv \int_0^\tau f^4(t)\mathcal{P}_{\text{g.s.}}(t)dt. \tag{25}$$

This yields $\tilde{T}^{(2)}_{\text{eff}}<35\tau/128$ for the effective interaction time and hence a larger cross section.

Figure 4 exhibits the influence of the peak intensity on our results for the total cross section for $I_0=5\times10^{14}$ and $3\times10^{15}$ W/cm$^2$, respectively. As expected, using $T^{(2)}_{\text{eff}}=35\tau/128$ reduces the result for the higher peak intensity, thereby suggesting a small but clearly noticeable intensity effect. However, this effect essentially disappears to within the thickness of the line when the depopulation of the initial state is properly accounted for through the effective interaction time $\tilde{T}^{(2)}_{\text{eff}}$.

Figure 5 shows the effect of the pulse length on the extracted results for the total cross section at a fixed laser intensity of $I_0=5\times10^{14}$ W/cm$^2$. For pulse durations larger than about six optical cycles, the probability for double ionization at the end of the pulse is directly proportional to the pulse length and, consequently, the effective interaction time. The cross section is then well defined and essentially no dependence on the length of the pulse remains after dividing the probability by $T^{(2)}_{\text{eff}}$. Hence, the time-dependent results become directly comparable to those obtained in time-independent or Floquet-type approaches. For short pulse durations (less than six optical cycles with the current parameters), on the other hand, the relationship between $\mathcal{P}_{kk}$ and the pulse length is no longer linear for the present parameters, and hence the extraction of a cross section using the formalism described above becomes meaningless.

### B. Triple-differential cross sections

Figure 6 displays the triple-differential cross section for two-photon DI of helium in a ten-cycle sine-squared laser pulse of central photon energy 42 eV and peak intensity $5\times10^{14}$ W/cm$^2$ for equal energy sharing ($E_1=E_2=2.5$ eV) of the two outgoing electrons. These results are for the co-

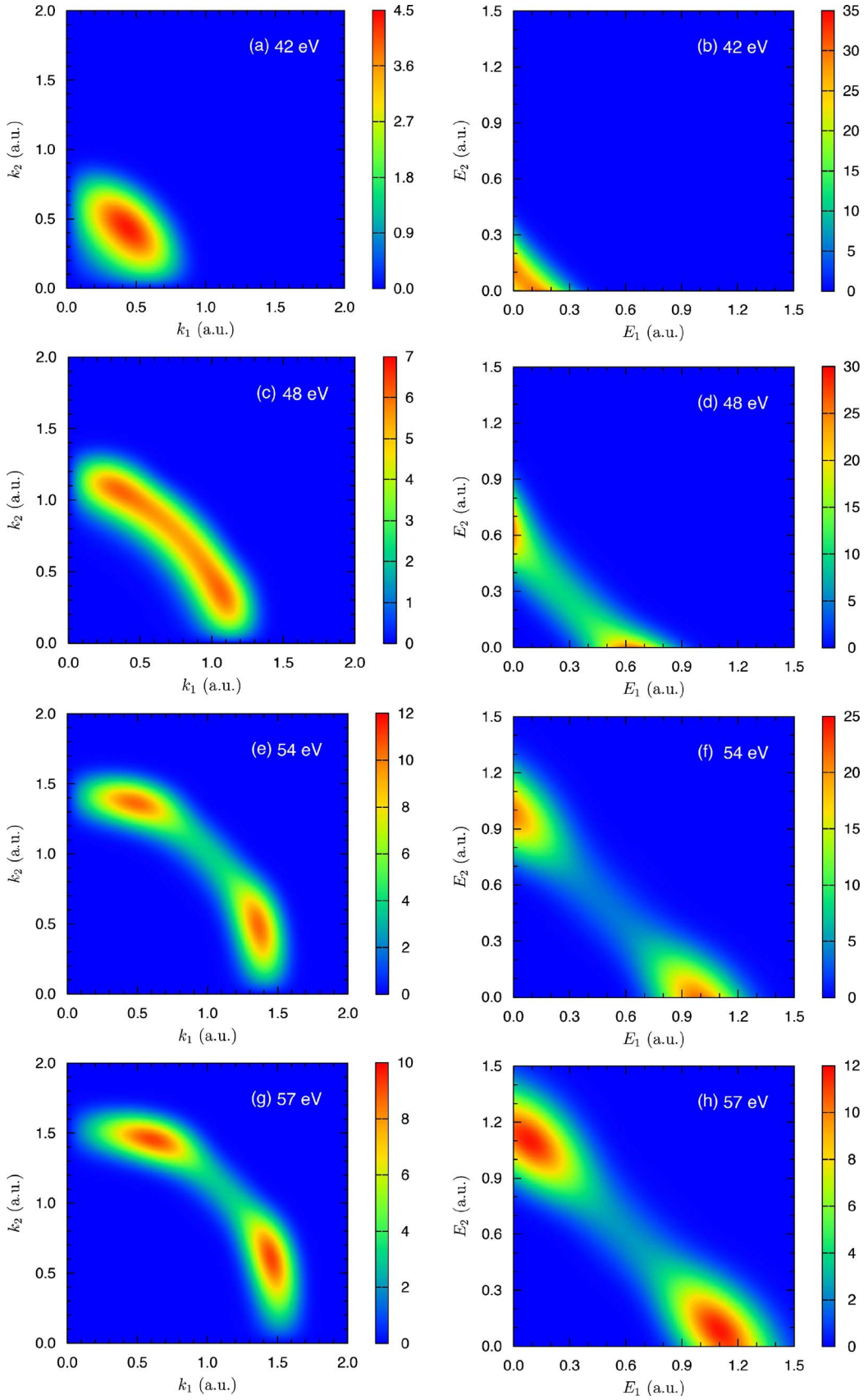


FIG. 8. (Color online) Momentum (left column) and energy (right column) distributions of the two escaping electrons. The laser pulse has a sine-squared envelope around the peak intensity of $5 \times 10^{14}$ W/cm$^2$ and a time duration of ten optical cycles. The central photon energies are 42, 48, 54, and 57 eV, respectively. The color bars are corresponding to units of $10^{-4}$ a.u.

planar geometry, where the electric field vector of the linearly polarized laser field and the momentum vectors of the two escaping electrons all lie in the same plane.

After once again multiplying the published results of Hu *et al.* [9] by 128/70 to account for the different definitions of $T_{\mathrm{eff}}$, the two sets of results obtained with the same maximum values $L_{\max}=l_{1,\max}=l_{2,\max}=3$ agree very well with each other, with only small differences in the heights of some of the maxima. Note that we compare with the results shown in Fig. 4 of Hu *et al.* [9]. These results were obtained using the time-dependent close-coupling (TDCC) approach [33], and they differ (slightly) from the results presented in Fig. 3 of the same paper. We also note that Ivanov and Kheifets [13] *divided* their TDCS results by 2.2 in order to achieve a better shape comparison with Hu *et al.* [9]. Hence, the *original* absolute values of Ivanov and Kheifets are in better agreement with our predictions, both for the total (see Fig. 3) and the triple-differential cross section.

Following a suggestion by Feist [27], we also checked the convergence of the results by increasing $l_{1,\max}$ and $l_{2,\max}$ to 4 and 5, respectively. Especially for the smallest TDCS values, when one of the electrons escapes at 90° relative to the laser polarization axis, the results change noticeably, i.e., the $(L_{\max},l_{1,\max},l_{2,\max})=(3,3,3)$ model is apparently not yet converged everywhere, with the most visible problem occurring for $\theta_1=90°$ and $\theta_2\approx 270°$. With our current computer code and the computational resources available to us, we cannot perform larger calculations, but the closeness of the (3,4,4) and (3,5,5) results suggests that the latter predictions are sufficiently converged that we would feel confident to compare them to experimental data if those became available. This conclusion is further supported by the work of Feist *et al.* [26], who were able to push the angular momenta even higher.

To provide additional information about out-of-plane geometries, Fig. 7 presents a three-dimensional (3D) impression for the triple-differential cross section for two-photon DI of helium. As in the previous figure, the direction of one of the escaping electrons is fixed with respect to the polarization axis of the laser field, but we are now plotting the probability for the other electron to escape into any direction. Having already looked at the coplanar cut of this figure, the strong dependence of the emission pattern on the fixed direction of one of these electrons is not surprising. It is clear that the two electrons try to avoid escaping in the same direction. In some cases, there is a tendency for escape on nearly opposite sides of the nucleus, but the details depend upon the direction between the laser polarization and the fixed momentum vector of one of the electrons. This indicates a comparable effect of the laser and the Coulomb fields. Overall, the two ionized electrons strongly prefer to escape along the polarization axis of the linearly polarized laser field. We hope that these detailed predictions will encourage experimentalists to test them as soon and in as much detail as possible.

Finally, we consider the momentum and the energy distribution of the two escaping electrons. Recall that Horner *et al.* [14] predicted a significant change in the total cross section already *below* the threshold for sequential double ionization at 54.4 eV. We therefore show our results for four different central photon energies (42, 48, 54, and 57 eV) in Fig. 8. At the lowest photon energy of 42 eV, we see an essentially flat distribution of the momenta and, correspondingly, the energies of the two escaping electrons. With increasing photon energy, but still below the threshold for sequential ionization, the probability that one of the two electrons takes essentially all the excess energy while the other takes none is strongly increasing, i.e., asymmetric energy sharing begins to dominate. At 57.0 eV, on the other hand, we see a clear signature of the sequential ionization mechanism. The excess energy of 1.29 a.u. is likely distributed in the way that one of the electrons takes 1.19 a.u., while the other takes 0.10 a.u. This corresponds to using the first photon to kick out one electron with a final energy of 57.0–24.6 eV, and the second photon to ionize $He^+(1s)$, yielding a free electron of energy of 57.0–54.4 eV (see Fig. 1). Nevertheless, some probability for other scenarios remains, indicating that the nonsequential double-ionization mechanism is still competing.

## IV. CONCLUSIONS

We have presented new calculations for two-photon double ionization of helium in a short, strong laser pulse. The distinguishing feature of our method is the use of a finite-element discrete-variable representation for the radial coordinates of the problem. Our results agree well with predictions from previous calculations, in which the cross sections were extracted by projecting the time-propagated wave function to an uncorrelated product of Coulomb functions. Our results for the various cross sections are numerically stable, and we have demonstrated that they neither depend on the pulse length nor on the laser intensity, as long as we are in the limit where the lowest nonvanishing order of perturbation theory should be valid. Previous findings to the contrary were apparently due to problematic definitions of the effective interaction time and the neglect of the initial-state depopulation in strong fields. In the future, we plan to extend the present work and investigate whether projecting on a correlated final state will change the results, as predicted by Foumouo *et al.* [12].

## ACKNOWLEDGMENTS

We thank Johannes Feist and James Colgan for many helpful discussions. We also thank H. Bachau, J. Colgan, B. Piraux, and H. W. van der Hart for sending us results in numerical form. X.G. and K.B. acknowledge support by the United States National Science Foundation under Grant No. PHY-0244470.

[1] M. Nagasono, E. Suljoti, A. Pietzsch, F. Hennies, M. Wellhöfer, J.-T. Hoeft, M. Martins, W. Wurth, R. Treusch, J. Feldhaus, J. R. Schneider, and A. Föhlisch, Phys. Rev. A **75**, 051406(R) (2007).
[2] R. Moshammer, Y. H. Jiang, L. Foucar, A. Rudenko, Th. Ergler, C. D. Schröter, S. Lüdemann, K. Zrost, D. Fischer, J. Titze, T. Jahnke, M. Schöffler, T. Weber, R. Dörner, T. J. M. Zouros, A. Dorn, T. Ferger, K. U. Kühnel, S. Düsterer, R. Treusch, P. Radcliffe, E. Plönjes, and J. Ullrich, Phys. Rev. Lett. **98**, 203001 (2007).
[3] V. Ayvazyan *et al.*, Eur. Phys. J. D **37**, 297 (2006).
[4] T. Laarmann, A. R. B. de Castro, P. Gürtler, W. Laasch, J. Schulz, H. Wabnitz, and T. Möller, Phys. Rev. A **72**, 023409 (2005).
[5] Y. Nabekawa, H. Hasegawa, E. J. Takahashi, and K. Midorikawa, Phys. Rev. Lett. **94**, 043001 (2005).
[6] R. Moshammer, D. Fischer, and H. Kollmus, in *Many-Particle Quantum Dynamics in Atomic and Molecular Fragmentation*, edited by J. Ullrich and V. Shevelko (Springer-Verlag, Berlin, Heidelberg, 2003), Chap. 2, p. 33.
[7] J. S. Parker, L. R. Moore, K. J. Meharg, D. Dundas, and K. T. Taylor, J. Phys. B **34**, L69 (2001).
[8] M. S. Pindzola, F. Robicheaux, S. D. Loch, J. C. Berengut, T. Topcu, J. Colgan, M. Foster, D. C. Griffin, C. P. Ballance, D. R. Schultz, T. Minami, N. R. Badnell, M. C. Witthoeft, D. R. Plante, D. M. Mitnik, J. A. Ludlow, and U. Kleiman, J. Phys. B **40**, R39 (2007).
[9] S. X. Hu, J. Colgan, and L. A. Collins, J. Phys. B **38**, L35 (2005).
[10] S. Laulan and H. Bachau, Phys. Rev. A **68**, 013409 (2003); S. Laulan, Ph.D. thesis, Université de Bordeaux I, 2004 (unpublished).
[11] L. Feng and H. W. van der Hart, J. Phys. B **36**, L1 (2003).
[12] E. Foumouo, G. L. Kamta, G. Edah, and B. Piraux, Phys. Rev. A **74**, 063409 (2006).
[13] I. A. Ivanov and A. S. Kheifets, Phys. Rev. A **75**, 033411 (2007).
[14] D. A. Horner, F. Morales, T. N. Rescigno, F. Martín, and C. W. McCurdy, Phys. Rev. A **76**, 030701(R) (2007).
[15] R. Shakeshaft, Phys. Rev. A **76**, 063405 (2007).
[16] H. Hasegawa, E. J. Takahashi, Y. Nabekawa, K. L. Ishikawa, and K. Midorikawa, Phys. Rev. A **71**, 023407 (2005).
[17] L. A. A. Nikolopoulos and P. Lambropoulos, Phys. Rev. A **74**, 063410 (2006).
[18] C. Bouri, P. Selles, L. Malegat, J. M. Teuler, M. Kwato Njock, and A. K. Kazansky, Phys. Rev. A **72**, 042716 (2005); C. Bouri, L. Malegat, P. Selles, and M. G. K. Njock, J. Phys. B **40**, F51 (2007).
[19] D. Proulx and R. Shakeshaft, Phys. Rev. A **48**, R875 (1993).
[20] R. C. Forrey, H. R. Sadeghpour, J. D. Baker, J. D. Morgan, and A. Dalgarno, Phys. Rev. A **51**, 2112 (1995).
[21] T. N. Rescigno and C. W. McCurdy, Phys. Rev. A **62**, 032706 (2000).
[22] C. W. McCurdy, D. A. Horner, and T. N. Rescigno, Phys. Rev. A **63**, 022711 (2001).
[23] C. W. McCurdy, M. Baertschy, and T. N. Rescigno, J. Phys. B **37**, R137 (2004).
[24] X. Guan, O. Zatsarinny, K. Bartschat, B. I. Schneider, J. Feist, and C. J. Noble, Phys. Rev. A **76**, 053411 (2007).
[25] A. R. Barnett, in *Computational Atomic Physics*, edited by K. Bartschat (Springer, Heidelberg, New York, 1996), Chap.9, p. 181.
[26] J. Feist, S. Nagele, R. Pazourek, E. Persson, B. I. Schneider, L.A. Collins, and J. Burgdörfer, Phys. Rev. A **77**, 043420 (2008).
[27] J. Feist (private communication).
[28] L. A. A. Nikolopoulos and P. Lambropoulos, J. Phys. B **34**, 545 (2001).
[29] L. A. A. Nikolopoulos and P. Lambropoulos, J. Phys. B **40**, 1347 (2007).
[30] Y. Nabekawa (private communication).
[31] D. A. Horner (private communication).
[32] B. Piraux, J. Bauer, S. Laulan, and H. Bachau, Eur. Phys. J. D **26**, 7 (2003).
[33] J. Colgan (private communication).